RSC Advances

PAPER

View Article Online
View Journal | View Issue

Cite this: *RSC Adv.*, 2017, **7**, 14640

Characterization of KOH modified biochars from different pyrolysis temperatures and enhanced adsorption of antibiotics†

Hua Huang,[a] Jingchun Tang,*[a] Kai Gao,[b] Ruozhu He,[a] Hang Zhao[a] and David Werner[c]

Poplar biochars from pyrolysis at temperatures of 300, 500 and 700 °C were modified with KOH and characterized by elemental analysis, Fourier transform infrared (FT-IR) spectroscopy, X-ray diffraction (XRD), and nitrogen adsorption–desorption isotherm studies. Adsorption experiments were carried out on the modified biochars to remove tetracycline (TC) from aqueous solution. The results showed that KOH modification could increase or decrease TC adsorption onto biochars depending on the different pyrolysis temperatures. Maximum adsorption capacities ($q_{e,m}$) of TC in modified biochar from a low pyrolysis temperature of 300 °C increased up to 21.17 mg g^{-1} relative to 4.30 mg g^{-1} in unmodified biochar of 300 °C (final TC concentrations were 8.83 and 25.70 mg L^{-1}, respectively). In contrast, $q_{e,m}$ decreased from 7.37 and 11.63 mg L^{-1} to 4.97 and 7.13 mg L^{-1} in biochars from higher pyrolysis temperatures of 500 and 700 °C with and without modification, respectively, even with an increase in S_{BET}. The adsorption ability of biochar can remain over a wider range of pH in modified biochar relative to unmodified biochar. Further analysis indicated that there was a strong linear regression relationship between $q_{e,m}$ and total functional oxygen groups using Bohem titration ($n = 6$, $R^2 = 0.84$), whereas no significant relationship was observed between $q_{e,m}$ and S_{BET} in this experiment. The result suggested that KOH modification of biochar from a low pyrolysis temperature can enhance TC adsorption and can be used over a wide range of pH, which may be a good choice for disposal of organic pollutants in aqueous solution.

Received 7th December 2016
Accepted 24th February 2017

DOI: 10.1039/c6ra27881g

rsc.li/rsc-advances

1 Introduction

Biochar is a solid product of the thermal pyrolysis of biomass, which is characterized by a large specific surface area, porous structure, enriched surface functional groups and mineral components.[1,2] With relative low production cost, abundant feedstock and favorable porous structure, it was considered to be an ideal alternative adsorbent for many environmental applications such as water treatment, soil remediation, soil improvement, and so on.[3,4] Recently, environmental pollution by antibiotics has received increasing attention. Among various antibiotics, tetracycline (TC) is most extensively used in the breeding industry to improve the yield of animal products. TC is scarcely metabolized by animals and recalcitrant in wastewater treatment plants (WWTPs), and will therefore eventually enter into aquatic and terrestrial environments.[5–7] As such, it is imperative to promote the treating capacity of TC by traditional WWTPs. Among various treatment options, the removal of TC from waste water by adsorption is a widely and easily used method. One critical point for this method is to find appropriate adsorbents with high adsorption capacity and low cost such as biochar. However, since TC is an ionic compound and negatively charged in environmental pH conditions, the adsorption capacity of untreated biochars for TC is very low,[8–11] which makes it necessary to modify the biochars to enhance their adsorption capacity.

Recently, efforts have been made to promote the adsorption capacity of biochars for specific pollutants. Due to low cost, good effectiveness and easy to operate, alkali treatment is an attractive modification method.[12] Overall, by enhancing surface oxygen functional groups (SOFGs), changing surface charges, removing ash and enlarging surface area (Fig. S1†), alkali modification increases the adsorption of biochar for metal cations,[13–15] metal anions[16] and various ionic organic compounds.[9,17,18] In addition, alkali modification could be used as the first step in a more complex modification process.[19] However, so far alkali modification was only conducted for biochars produced at a fixed pyrolysis temperature, and studies

[a]*Key Laboratory of Pollution Processes and Environmental Criteria (Ministry of Education), Tianjin Engineering Center of Environmental Diagnosis and Contamination Remediation, College of Environmental Science and Engineering, Nankai University, 94 Weijin Road, Tianjin 300071, China. E-mail: tangjch@nankai.edu.cn; Fax: +86 2283614117; Tel: +86 2283614117*

[b]*Tianjin Academy of Environmental Science, Tianjin 300191, China*

[c]*School of Civil Engineering and Geosciences, Newcastle University, Newcastle upon Tyne, NE1 7RU, UK*

† Electronic supplementary information (ESI) available. See DOI: 10.1039/c6ra27881g

comparing alkali modification effects on biochars from different pyrolysis temperatures are still lack.

For biochars, pyrolysis temperature is one of the most important operating parameters that control product characteristics and the yield rate.[1,20] With increasing pyrolysis temperature, it was found that nonpolar, specific area, pore volumes and aromaticity increase whereas raw biomass features, functional groups, volatile substances, hydrophilicity and yield rates of BC decrease.[21,22] In previous studies, middle or high temperature biochars were selected for KOH treatment, which may be due to higher specific area and aromaticity. Indeed, it was confirmed that high temperature sugarcane bagasse biochar adsorbed more TC than that from low temperature due to stronger π–π EDA interactions between TC and graphitized surfaces.[8] However, from the view of both modifying and adsorption mechanisms, it seemed that low temperature pyrolysis biochars are also potential for KOH treatment to improve TC adsorption capacity because that alkali treatment could catalyze hydrolysis of lignocellulose left in low temperature biochars and produced more SOFGs.[15,23,24] Furthermore, it may promote TC binding to hydroxyl group or ionized moiety of biochars by n–π EDA interactions (Fig. S2†).[19] As well known, cost of BC increased with elevated pyrolysis temperature but yield decreased. Therefore, it was important to compare the influence of pyrolysis temperature on KOH modifying processes.

The primary objective of this work is to investigate the effect of alkali treatment (KOH) on the characteristics of polar wood biochars produced at three representative pyrolysis temperatures, *i.e.* 300 °C, 500 °C and 700 °C. The modification effect on the adsorption of tetracycline was also compared by studying adsorption kinetics, adsorption isotherms and adsorption mechanism.

2 Materials and methods

2.1 Raw materials

Poplar sawdust was supplied by the Taiyuan wood-working factory (Tianjin). Before use, sawdust was crushed and sieved into 0.15–0.30 mm. TC (purity > 98.0%) was purchased from DingGuo Biotech Co., Ltd. (Tianjin). All other chemicals used in the experiment were analytical grade.

2.2 Biochars preparation and modification

Raw biochars were prepared by an oxygen limited pyrolysis method in a muffle furnace. Briefly, around 90 g raw sawdust was compacted in a 250 mL ceramic pot enveloped with aluminum foil, and pyrolyzed in a muffle furnace at 300, 500 and 700 °C, respectively. Pyrolysis time was fixed at 6 h. Raw biochars were named as RBCs (RBC300, RBC500 and RBC700, respectively). The yields of each biochars were 50.88%, 29.40% and 23.50%, respectively.

The KOH modification process was conducted as follows: 10 g of RBCs were placed in beakers, 100 mL 2 mol L^{-1} KOH solution was added, and stirred for five hours at 65 °C. Then the biochars were washed 10 times (0.5 h per time) in 500 mL warm deionized water (50 °C) with stirring. Then dried at 60 °C for 24 h and stored in a desiccator. The modified biochars were referred as KBCs (KBC300, KBC500 and KBC700, respectively).

2.3 Characterization of biochar samples

The element (carbon, C; hydrogen, H; and nitrogen, N) composition was analyzed with an elemental analyzer (Vario EL cube, Elementar Analysensysteme GmbH, Hanau, Germany), and the O content was calculated on the basis of mass difference. Ash content was measured by heating the samples at 750 °C for 6 h.

Scanning electron microscopy (SEM) (Shimadzu SS-550, Shimadzu Corp., Kyoto, Japan) was carried out to observe the surface morphologies of the samples. The pore structure characteristics of the samples were determined by N_2 adsorption at 77 K using a surface area analyzer (ASAP 2020/Tristar 3000, Micromeritics Instrument Corp., Georgia, USA). The specific surface area was calculated following the multipoint N_2-Brunauer–Emmett–Teller (BET) adsorption method.[25,26] The volume and surface area of the micropores were obtained using the BJH (Barrette–Joynere–Halenda) method.[27]

The functional groups of the samples were identified using Fourier transform infrared spectroscopy (FTIR, FTS6000, Bio-Rad Corp., California, USA) in the wavenumber range of 4000–400 cm^{-1}. The inorganic components were identified by X-ray diffraction (XRD) (Bruker AXS GmbH, Karlsruhe, Germany) with Cu Kα radiation ($\lambda = 1.5406$ Å). Scan speed, step size and 2θ range were 10° min^{-1}, 0.02° and 10–65°, respectively. The pH values of zero point charges (pH_{PZC}) of biochar samples were measured as described by Liu *et al.* (2011).[28] Oxygen-containing functional groups were examined by the Bohem titration method.[29,30]

2.4 Sorption experiments

Batch adsorption experiments were conducted at 298 K. First, 40 mL glass screw bottles (CNW Technologies, Germany) were carefully wrapped with aluminum foils to prevent photolysis of TC. TC of specific concentrations was prepared in 0.01 mol L^{-1} $NaNO_3$ as background solution, and pH was adjusted to 5.0 with 0.1 mol L^{-1} NaOH and HNO_3. After addition of the adsorbents and adsorbates, bottles were agitated by end-over-end rotation for presupposed times. Samples obtained were filtered through 0.45 μm polytetrafluoroethylene (PTFE) microporous membranes. Finally, the TC concentrations of filtrates were determined by a spectrometer method using an ultraviolet-visible detector at 360 nm (TU-1950, Puxi testmart Corp., China).

For measuring adsorption kinetics, variable amounts of adsorbents (40–80 mg) were placed into glass bottles with 40 mL TC solution (30 mg L^{-1}), then harvested at time intervals of 2–312 h. The adsorbed amount of TC at t time, q_t (mg g^{-1}), was determined according to eqn (1):

$$q_t = \frac{(C_0 - C_t)V}{m} \quad (1)$$

where C_0 and C_t are liquid phase concentrations of TC (mg L^{-1}) in filtrate at the start and time t, respectively, V is the volume of TC solution (L), and m is the dry mass of adsorbents used (g).

TC solutions of 10–50 mg L^{-1} were used in adsorption isotherm equilibrium studies. Due to the relatively high adsorption capacity, an extra TC solution (90 mg L^{-1}) was set up

for KBC300. According to the results of the adsorption kinetics, agitation time was set at 72 h. The adsorbed amount of TC, q_e (mg L^{-1}), was calculated by the following equation:

$$q_e = \frac{(C_0 - C_e)V}{m} \quad (2)$$

where C_0 and C_e are the initial and 72 h liquid phase concentrations of TC (mg L^{-1}) in filtrate, respectively, V is the volume of TC solution (L), and m is the dry mass of adsorbents used (g).

Pseudo-first order, pseudo-second order, intraparticle diffusion and Elovich models were used for simulating the adsorption kinetics. Freundlich and Temkin models were used for simulating adsorption isotherm data. These models and relevant parameters were detailed in Table S1.†

Correlation coefficients (R^2) and normalized standard deviations, Δq_e (%), were used to determine the best model to fit the experimental data.[31] Δq_e was calculated by following equation:

$$\Delta q_e(\%) = 100\sqrt{\sum \frac{\left[\left(q_{e,exp} - q_{e,calc}\right)/q_{e,exp}\right]^2}{N-1}}$$

where N is the number of data points, $q_{e,exp}$ and $q_{e,calc}$ are experimental and calculated adsorption capacity, respectively.

To study the influence of pH on TC adsorption, adsorbents were buffered in TC solutions with different pH (3.1, 4.0, 4.9, 5.9, 7.0, 8.1 and 9.1). The TC concentration, temperature and agitation time were fixed at 30 mg L^{-1}, 298 K and 72 h, respectively.

3 Results and discussion

3.1 Bulk properties of biochars

The elemental contents of the biochars are presented in Table 1. With the increase of pyrolysis temperature, C content increased, and H and O decreased in both RBCs and KBCs. These variations have been reported by earlier studies, and were assigned to dehydration and carbonization reactions.[21,32] After KOH treatment, O contents of biochars were keenly reinforced, increasing from 19.95%, 7.09% and 1.22 to 27.7%, 10.06% and 5.96% for KBC300, KBC500 and KBC700, respectively. The obvious improvement of O content was thought to be contributed from two major reasons: firstly, KOH treatment largely removed the ash from the carbon materials which resulted in low ash content. Secondly, surface oxygen functional groups (SOFGs) of biochars could be considerably enhanced by KOH modification,[13,17] and were evidenced by FT-IR and Bohem titration exhibited later. KOH treatment also altered C contents of biochars and increased H contents. It was observed that C of KBC300 was lower than that of RBC300, whereas higher C content was found in KBC700 relative to RBC700. This was because that KOH treatment removed more non-fixed carbon from RBC300 at low temperature,[33,34] and on the contrary, more ash from RBC700 was removed at higher temperature which resulted in increased C content.

The ash content in RBCs and KBCs is presented in Table 1. It was found that ash content increased gradually from 3.21% for the feedstock to 12.09% for RBC700. This was because that components like hemicellulose, cellulose and part of lignin was destroyed during thermal decomposition while mineral substances remained and increased relatively. This trend was in consistent with other studies.[21,32] As for the KBCs, changing trend of ash content with pyrolysis temperature was reversed, with KBC700 showing the lowest ash content. It is well known that KOH can react with SiO_2 to form silicate ($2KOH + SiO_2 \rightarrow K_2SiO_3 + H_2O$), which will be flushed away through washing.[9] When pyrolysis temperature increased, the surface area of biochars increased correspondingly. Larger surface area facilitated contacting with KOH solution and would also improve the washing effect. Therefore, ash contents of RBC300 merely decreased from 5.95% to 4.34% of KBC300, whereas the values of RBC700 dramatically decreased from 12.09% to 2.79% of KBC700.

3.2 Surface properties of biochars

The effect of pyrolysis temperatures and KOH treatments on the porous surface structure of biochars were studied by SEM and BET method in Fig. S3† and Table 1, respectively. The raw feedstock of poplar sawdust was a plated structure with few pores, and surfaces of biochars became rough after pyrolysis. Through removing ash, tar particles and corrosion of hydrolysis reactions of KOH treatment, wrinkles appeared on KBC300 and KBC500 which made surface rougher. This was in line with previous studies.[9,14] An interesting phenomenon was that small

Table 1 Effects of pyrolysis temperatures and KOH treatments on the property of biochars[a]

	Elemental analysis (wt%)						
	C	H	O	Ash%	pH_{PZC}	S_{BET} m^2 g^{-1}	V_{total} cm^3 g^{-1}
Feedstock	48.7 ± 1	6.3 ± 0.2	41.8 ± 1.2	3.21	ND	ND	ND
RBC300	70.3 ± 0.2	3.8 ± 0.3	20 ± 0.1	5.95	8.62	—	—
RBC500	84.5 ± 1.1	1.0 ± 0.3	8.5 ± 1.4	6.05	9.78	12.32	0.004
RBC700	86 ± 0.1	0.7 ± 0.3	1.2 ± 0.4	12.09	10.68	111.39	0.008
KBC300	64 ± 0.2	3.9 ± 0.2	27.7 ± 0.1	4.34	8.41	1.61	0.002
KBC500	84.7 ± 1	1.9 ± 0.5	10.1 ± 1.5	3.36	9.52	106.8	0.006
KBC700	90.5 ± 0.2	0.8 ± 0	6 ± 0.2	2.79	9.26	337.81	0.024

[a] (a) Nitrogen content was too low to be detected; (b) oxygen content is estimated as follows: O = 100% − (C% + H% + ash%); (c) S_{BET} and V_{total} of RBC300 was too low to be determined; (d) pH_{PZC}, S_{BET} and V_{toal} of feedstock were not measured.

bubbles formed on the surface of RBC700, which may contributed to volatile gas formed during high temperature pyrolysis process (>600 °C) and not released.[33,35] KOH treatment punctured the bubbles and new pores formed. This make surface of KBC700 was the roughest in this experiment. Both V_{total} and S_{BET} of KBC700 were greatly increased (from 106.80 $m^2\ g^{-1}$ to 337.81 $m^2\ g^{-1}$ for S_{BET}, and from 0.008 $cm^3\ g^{-1}$ to 0.024 $cm^3\ g^{-1}$ for V_{total}), whereas only S_{BET} were improved for KBC500 (from 12.32 $m^2\ g^{-1}$ to 111.39 $m^2\ g^{-1}$ for S_{BET}, and from 0.004 $cm^3\ g^{-1}$ to 0.006 $cm^3\ g^{-1}$ for V_{total}). However, the S_{BET} value is low in both RBC300 and KBC300, indicating that surface area did not have a great increase after KOH modification in biochar from low pyrolysis temperature.

The evolution of FT-IR spectra of feedstock and biochars is illustrated in Fig. 1. In order to semi-quantitatively investigate effects of KOH treatment on functional groups of RBCs, normalization of data based on 2918 cm^{-1} ($-CH_2$) for biochars at 300 °C and 500 °C, and 1651 cm^{-1} (C=C) for 700 °C were conducted according to Chen *et al.* (2016).[36] After heating at 300 °C, –OH, aliphatic C–H and C–O stretching vibrations at 3500–3200, 2945/2885 and 1110/1030 cm^{-1} declined strongly, indicating decomposition of cellulose, hemicellulose, and lignin contents. Meanwhile, the absorbance of aromatic C–H, carboxyl C=O and aromatic C=C (and/or C=O of quinones or conjugated ketones) at 3050, 1720 and 1600 cm^{-1} enhanced considerably, reflecting the formation of carboxylic C, ketones, esters, anhydrides and/or aromatic components, and occurrence of strong dehydration reaction and carbonization at 300 °C. With respect to RBC300, –OH, aliphatic C–H and C–O stretching vibrations of RBC500 at 3500–3200, 2945/2885 and 1030 cm^{-1} decreased, and aromatic C–H and carboxyl C=O at 3050 and 1600 cm^{-1} increased. This attributes to an increasing degree of condensation at 500 °C pyrolysis. At 700 °C, most features of biomass were eliminated with the loss of polar groups and condensation of aromatic units,[37] which is conformity with findings of Kuiluweit *et al.* (2012).[21]

For KOH modification, it was unexpectedly found that –OH at 3340/3365 cm^{-1} increased in KBC300 but declined in KBC500. It appeared that KOH modification process could improve –OH around 3320–3350 cm^{-1} in a hydrothermal carbonization process.[13,15] This phenomenon could be explained by the fact that KOH catalyzed the cleavage of ether linkages in lignin,[15,24] which was confirmed by reduction of C=C stretching at 1510 and 1440 cm^{-1} (indicative of lignin).[21] For moderate temperature of 500 °C, it was found that KOH treatment could either decrease –OH (3418 cm^{-1}) for a commercial fast pyrolysis biochars,[9] increase –OH (3352 cm^{-1}) for municipal solid wastes biochar,[16] or keep stable –OH for bamboo biochar.[38] It seemed that effects of alkali treatment on –OH formation of biochars was depended on various factors considered that these biochars all prepared around 500 °C with different feedstocks, charring methods and conditions of alkali treatment. As for the other functional groups, KOH treatment only improve absorbance intensity at 3050 cm^{-1} (aromatic C–C) for KBC300 and at 1720 cm^{-1} (COOH) for KBC500, and diminished Si–O–Si at 1041 cm^{-1} both for KBC300 and KBC500. The plain spectra in both RBC700 and KBC700 suggested that the functional groups was almost eliminated in biochars of high pyrolysis temperature.

The X-ray diffraction patterns of poplar wood and its biochars are shown in Fig. 2. Two broad peaks at $2\theta = 16.49°$ and 22.48° of raw wood sawdust were detected, which were assigned to typical diffraction peaks of the plane (101) and (002) of cellulose crystalline.[39,40] After pyrolysis at 300 °C, the intensity of these 2 peaks declined, which illustrates the disappearance of cellulose crystallinity. When further raising pyrolysis temperature to 500 °C, broad peaks at $2\theta = 22.85°$ and 43.17° emerged, which became narrow at 700 °C showing the formation of turbostratic crystallites according to Keiluweit *et al.*, (2010) and Tongpoothorn *et al.* (2011).[21,41] Some small peaks also appeared in RBCs, such as $2\theta = 26.80°$, 27.70°, 29.20°, 49.88°, 50.34° and 50.93°, which became smaller or disappeared after KOH treatment. It is convinced that the peak 2θ at 26.80° was SiO_2 [*hkl* (011)], and the other peaks were speculated to be some other mineral impurities. Thus, the results of XRD confirmed that KOH treatments could remove impurities from RBC biochars, while part of SiO_2 was still left.

3.3 Tetracycline adsorption on biochars

3.3.1 Adsorption kinetics. Kinetic adsorption of TC by RBCs and KBCs is depicted in Fig. 3. It was found that adsorption of TC by biochars was very slow, and adsorption

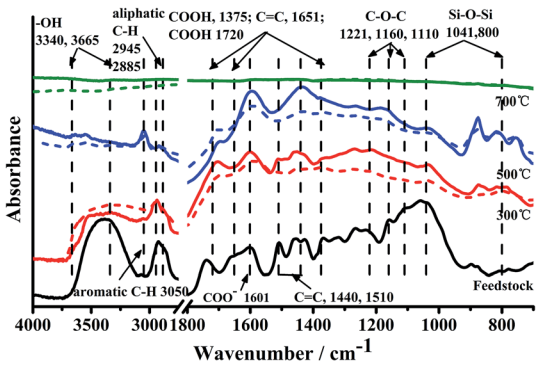

Fig. 1 FT-IR spectra of feedstock (black solid line) RBCs (colored solid lines) and KBCs (colored dash lines). Data transformation were done based on $-CH_2$ (2918 cm^{-1}) for RBC300, RBC500, KBC300 and KBC500, and on 1651 cm^{-1} (C=C) for RBC700 and KBC700, respectively.

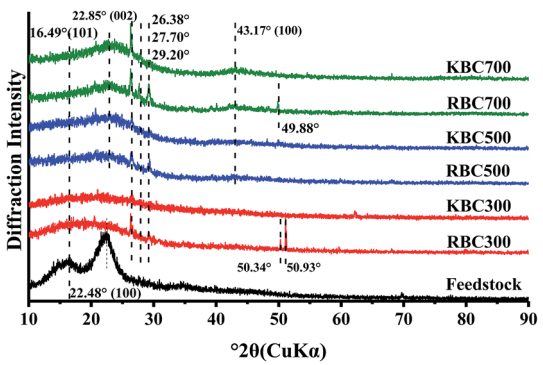

Fig. 2 X-ray diffractogram of RBC and KBC biochars.

equilibrium achieved at 264 h for RBCs. KOH treatment enhanced the TC adsorption with faster equilibrium times of 216 h, 120 h and 168 h for KBC300, KBC500 and KBC700, respectively. This result comports with that of Liu *et al.* (2012).[9] The maximum equilibrium adsorption capacities ($q_{e,m}$) increased with elevated pyrolysis temperatures for RBCs with the values of 4.30, 7.37 and 11.63 mg g^{-1} for RBC300, RBC500 and RBC700, respectively. The $q_{e,m}$ of KBC300 was 21.17 mg g^{-1}, a 392.3% increase relative to RBC300, whereas, KBC500 and KBC700 $q_{e,m}$ values were declined to 4.97 mg g^{-1} and 7.13 mg g^{-1}, respectively.

To better understand adsorption kinetics of TC onto biochars, pseudo-first order, pseudo-second order, Elovich and interparticle diffusion models were employed to simulate the experimental data and the results were exhibited in Fig. 3. The kinetic parameters are listed in Tables S2 and S3.†

According to Table S2,† the Elovich model was the most suitable model to match the experimental data of RBC300, RBC700, KBC300 and KBC700, with R^2 and Δq_e values in the range of 0.97–0.99 and 2.30–11.12%, respectively. For RBC500 and KBC500, R^2 of the pseudo-second order model was higher than that of the Elovich model (0.95 *vs.* 0.91 for RBC500, and 0.97 *vs.* 0.96 for KBC500), and Δq_e were lower for the Elovich model as compared to the pseudo-second order model (14.26% *vs.* 27.52% for RBC500, and 9.92% *vs.* 16.03% for KBC500). This means pseudo-second order model was more appropriate to describe the adsorption kinetics process of RBC500 and KBC500. Pseudo-second order model is based on the assumption that chemisorption is the rate-limiting step.[42] Elovich model is an empirical equation which assumes that adsorbent surface is heterogeneous, and both desorption or interactions between adsorbed species could affect the adsorption kinetics at low surface coverage. Furthermore, it is also on the basis of chemisorption assumption.[31,43] Therefore, chemisorption appeared to be the primary mechanism for TC adsorption by RBCs and KBCs (Fig. S2†). Meanwhile, adsorption and desorption of TC happened simultaneously for RBC300, RBC700, KBC300 and KBC700. As to pseudo-first order model, it was not suitable for the data in this experiment.

A further parameter comparison was conducted with pseudo-second order model due to the lowest Δq_e = 12.92% (n = 132). With pyrolysis temperature increasing, k_2 of RBCs increased from 0.018 to 0.084 g mg^{-1} h^{-1}, and h_0 increased from 0.307 to 11.284 mg g^{-1} h^{-1}, which means that the TC adsorption rate by RBCs increased with pyrolysis temperature.[5] This conclusion was obtained by parameter comparison and was consistent with the result of Zhou *et al.* (2016) who found that Cr(VI) adsorption rate also increased with pyrolysis temperature increase.[44] As to KOH modification, it increased k_2 and h_0 values of KBC300 whereas decreased that of KBC500 and KBC700.

The intraparticle diffusion model, which assumes that the adsorption mechanism occurs *via* the diffusion of adsorbate molecules into the pores of adsorbent material, is used to determine the rate-limiting step of the adsorption process.[43,45] By transforming t into $t^{0.5}$, the non-linear t–q_t adsorption kinetics relationship was changed to a linear $t^{0.5}$–q_t relationship in Fig. 3c and d. Polyline curves observed in whole adsorption process revealed that intraparticle diffusion was not the unique mechanism governing the TC adsorption process. Nevertheless, three distinct turning points could divide all curves into three linear parts were also discerned. According to Martins *et al.* (2015),[43] these linear parts corresponds to three phases of adsorption kinetics processes: the first phase represents a fast diffusion of TC to the external surface of biochars; in the second phase intraparticle diffusion is the rate-limiting step and the line slope corresponds to the intraparticle diffusion constant (k_{id}), whereas the intercept value (C_i) gives information about the thickness of the boundary layer; as to the third phase, the linear dependency approximation of the concentration on $t^{0.5}$ no longer holds.

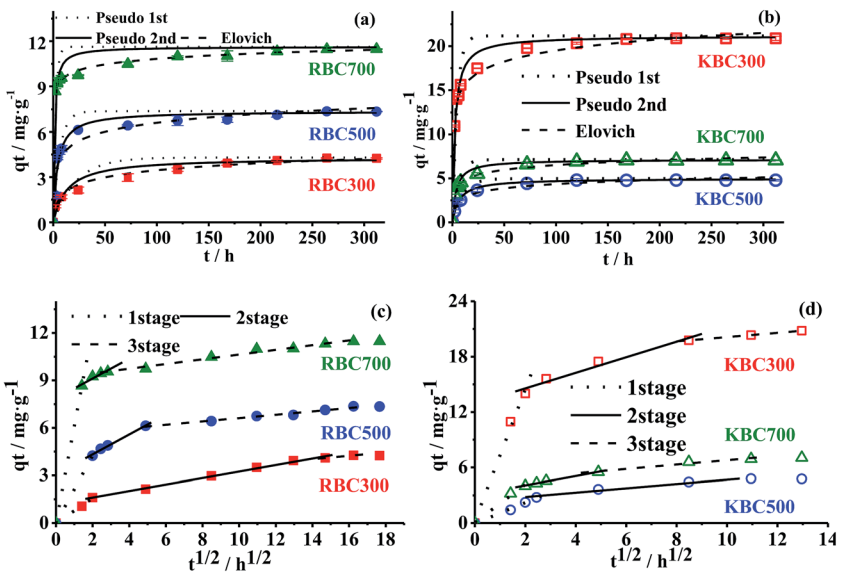

Fig. 3 Experimental data of adsorption kinetic and non-linear fitting of pseudo-first order, pseudo-second order and Elovich models for TC adsorption of RBCs (a) and KBCs (b), and intraparticle diffusion models for RBCs (c) and KBCs (d).

Since the first stage of the intraparticle diffusion happened fast, and R^2 of the third stage was too low, just the second stage was further studied and parameters are shown in Table S3.† For RBCs, k_{id} increased from 0.195 to 0.766 mg g^{-1} $h^{-0.5}$, C_i increased from 1.260 to 7.620 mg g^{-1}, and the duration time decreased from 116 to 6 h correspondingly. It suggested that the intraparticle diffusion rate at the second stage increased with pyrolysis temperature, and the thickness of the boundary layer became larger. Compared with RBC300, k_{id} of KBC300 increased from 0.195 to 0.842 mg g^{-1} $h^{-0.5}$, C_i increased from 1.260 to 12.882 mg g^{-1}, and duration time decreased from 116 to 68 h. On the contrary, k_{id} of KBC500 and KBC700 decreased from 0.630 and 0.766 to 0.234 mg g^{-1} min^{-1} and 0.345 mg g^{-1} min^{-1}, C_i decreased to 2.342 mg g^{-1} and 3.644 mg g^{-1}, respectively. This result illustrates that KOH treatment accelerated intraparticle diffusion process for KBC300, whereas it slowed down the diffusion for KBC500 and KBC700.

3.3.2 Adsorption isotherms. The non-linear fitting results of adsorption isotherms are depicted in Fig. 4 and the parameters are detailed in Table S4.†

Except for KBC300 (R^2 = 0.77 and Δq_e = 20.31%), the Freundlich model was appropriate for the experimental data of the other five biochars, with R^2 and Δq_e ranging from 0.96–0.99 and 2.73–7.03%, respectively. The Freundlich model is an empirical equation based on sorption on a heterogeneous surfaces and assumes that sorption strength declines with consuming occupation of sorption sites.[31,46,47] The parameter, $1/n_F$, provides information related to the surface heterogeneity, which is closer to zero when the material surface is more heterogeneous.[43] For RBCs, $1/n_F$ decreased with pyrolysis temperature raising. This trend was consistent with Cr(VI) adsorption to biochars.[44] $1/n_F$ of KBC500 and KBC700 were lower than that of RBC500 and RBC700, respectively, which implied that both increase of pyrolysis temperature and KOH treatment could enhance the heterogeneity of biochars' surface. Furthermore, this result was in conformity with variation of surface as exhibited in SEM.

The Temkin model assumes that the adsorption heat of adsorbate molecules declines linearly with the coverage of adsorbent due to adsorbent–adsorbate interactions. In this model, the Temkin constant (b_T) indicates whether the adsorption reaction is exothermic ($b_T > 1$) or endothermic ($b_T < 1$).[46] According to Table S4,† the Temkin model was suitable to describe experimental data for all adsorbents, with R^2 and Δq_e ranging from 0.90–0.98 and 2.68–12.63%, respectively. The b_T values of biochars were in the range of 187.8–1731.9, implying that adsorption of TC onto biochars occurs exothermically. It also suggests that electrostatic interaction and/or the heterogeneity of pores on the biochars surface plays a vital role in TC adsorption.[5] The b_T values of RBCs decreased with pyrolysis temperature, which implies adsorption energy of TC to biochars decreased with elevation of pyrolysis temperature. The b_T values of KBC500 and KBC700 were higher than that of RBC500 and RBC700, whereas the value of KBC300 was lower than that of RBC300. It implied that KOH treatment decreased adsorption energy at 300 °C and increased adsorption energy at 500 °C and 700 °C in this experiment, which is in consistence with the adsorption result.

3.4 The promotion mechanism

As displayed above, KOH treatment promoted TC adsorptive properties of KBC300 with lowest S_{BET}, whereas decreased that of KBC500 and KBC700 with higher S_{BET}. It implied that q_e of TC was independent on biochars surface area in this work. Thus, it was speculated that increasement of SOFGs was mainly responsible for enhancement of TC adsorption by KBC300.

To verify this hypothesis, SOFGs of biochars were quantitatively examined with Bohem titration. As showed in Fig. S4,† alkalic SOFGs of RBCs increased from 5.44 to 6.50 mmol g^{-1} with pyrolysis temperature increasing whereas acidic SOFGs (0.01–0.70 mmol g^{-1}) diminished gradually. After KOH treatment, acidic, alkalic and total SOFGs of KBC300 all increased from 0.70, 5.44 and 6.14 mmol g^{-1} to 1.71, 6.50 and 8.21 mmol g^{-1}, respectively. However, SOFGs in KBC500 and KBC700 both decreased as compared to raw biochars at these respective pyrolysis temperatures. Comprehensively considered the results of FT-IR, Bohem titration and dissociation constants (pK_a) of SOFGs, the formation of phenolic –OH ($pK_a > 10.25$) from lignin (see Fig. S1†) mainly contributed to enhancement of SOFGs.[36] Furthermore, linear regression between total SOFGs determined by Bohem titration and $q_{e,m}$ in the kinetics adsorption experiment was conducted and is depicted in Fig. 5. The R^2 of linear equation was 0.84 within all 6 biochars (n = 6) and was further increased up to 0.97 when linear regression was repeated without RBC300 (n = 5). This result demonstrates a strong positive linear relationship between SOFGs and $q_{e,m}$. On the contrary, there was no significant relationship between S_{BET} and $q_{e,m}$ in this experiment.

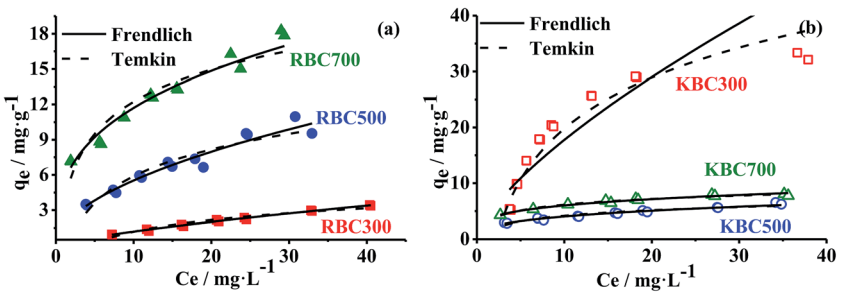

Fig. 4 Experimental data of adsorption isotherm and the non-linear fitting of Freundlich (red solid line) and Temkin (blue dash line) models for RBCs (a) and KBCs (b).

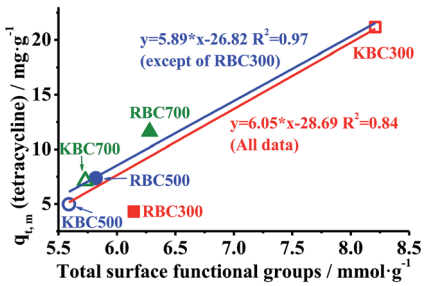

Fig. 5 Relationship between total surface functional groups and TC adsorption amounts.

In an earlier study, Jing *et al.* (2014) found that n–π EDA interaction was responsible for the elevated TC adsorption affinity of the NaOH–methyl alcohol modified char, which characterized by augment of hydroxyl group.[19] In this interaction, hydroxyl group (–OH) or ionized moiety ($–O^-$) of biochars act as n-electron donor and conjugated enone structures of TC behaves as electron-depleted sites to withdraw/accept electron. Therefore, we proposed that improvement of hydroxyl groups *via* KOH catalyzing hydrolysis reaction, and enhancement of n–π EDA between hydroxyl and TC was the main mechanism for promotion of TC adsorption by KBC300 (referred as promotion mechanism).

3.5 Influence of pH on TC adsorption

The pH point of zero charges (pH_{PZC}), which measures total (outside and internal) surface charges and relates to the capacity of materials to release/uptake protons,[48] was determined by curves detailed in Fig. S5† and values in Table 1. It was found that all pH_{PZC} of biochars were higher than 8.5, and increased with pyrolysis temperature. KOH treatment deceased pH_{PZC} by 0.21–1.42 pH units, which was consistent with the result of Liu *et al.* (2012).[9] The pH_{PZC} of biochars is very important for ionic compounds adsorption, as it determines the nature of the electrostatic attraction and repulsion between biochars and adsorbates.

Since TC is an amphoteric molecule with three pK_a values (3.3, 7.7 and 9.7), TC can exist as a cation (+00), zwitterion (+-0) or anion (+-/0-) when pH is in the ranges of ~3.3, 3.3–7.7 and 7.7~ (Fig. S6†), respectively. Previous studies have confirmed that TC adsorption on porous carbon materials are mainly depended on π–π EDA interaction and cation–π bonding,[19,49] and a lumped term for all other interactions, including n–π EDA interaction, H-bonding, electrostatic interaction, surface complexation and van der Waals forces.[9,50,51] The pH value influence not only electrostatic interaction by altering charges of TC and biochars but also electron acceptor ability and dissociation of amino groups of TC, which finally affected π–π EDA interaction, n–π EDA interaction and cation–π bonding.[5,49]

The dependences of the amount of TC sorbed onto biochars on variable initial pH (3–9) were depicted in Fig. 6. Due to the equilibrium pH (pH_{eqm}), rather than initial pH, influencing TC adsorption eventually,[9] the pH_{eqm} was plotted as the relevant variable on the *x* axis. All pH_{eqm} were below the pH_{PZC} of each biochars and above the $pK_{a1} = 3.3$ of TC. For RBC300, there were two stages for decrease of q_e: the first stage was at $pH_{eqm} = 6.81$–7.65, which was near $pK_{a2} = 7.7$ of TC. At this stage, electron acceptor ability of the enol of TC diminished as a consequence of deprotonation of phenolic diketone (C-10:C-11:C-12).[5] Correspondingly, q_e decreased from 6.32 to 4.22 mg g^{-1} attributed to reduction of π–π EDA interaction between TC and RBC300. The second stage was at $pH_{eqm} = 7.65$–8.10, which was just below the pH_{PZC} of RBC300 (8.62). At this stage, most protons of biochars were released into aqueous phase and make RBC300 more negatively charged. Due to increasing electrostatic repulsion, q_e decreased to as low as 0.45 mg g^{-1}.[10,50] For RBC500, the first stage was not displayed since pH_{PZC} was always higher than TC pK_{a2}. The second stage for RBC500 was in $pH_{eqm} = 8.94$–9.46. Since pH_{PZC} of RBC500 was 9.78, which also coincides with the $pK_{a3} = 9.7$ of TC, the dramatic decrease of q_e could result from either electrostatics repulsion between negative charged TC and BC, or the decrease of cation–π bonding. As for the RBC700, q_e was kept constant up to $pH_{eqm} = 9.76$ and less pH influence was observed around pK_{a2}, which was indicative of less contribution of electrostatic interactions. This was consistent with the result of the least surface oxygen functional groups (SOFGs) in RBC700 and was in line with Li *et al.* (2016).[8] Considerable decrease of q_e happened between $pH_{eqm} = 9.16$–10.15 because of the deprotonation of dimethylamine (C-4) groups of TC which reduced cation–π bonding between RBC700 and TC molecules.[5]

After KOH treatment, impact of pH on TC adsorption by KBCs was reduced relative to that of RBC. Although q_e of KBC300 also decreased from 24.95 to 20.54 mg g^{-1} along with pH increasing, no apparent turning points were observed near pK_{a2} of TC, and the extent of the reduction (17.7% *vs.* 93.7%)

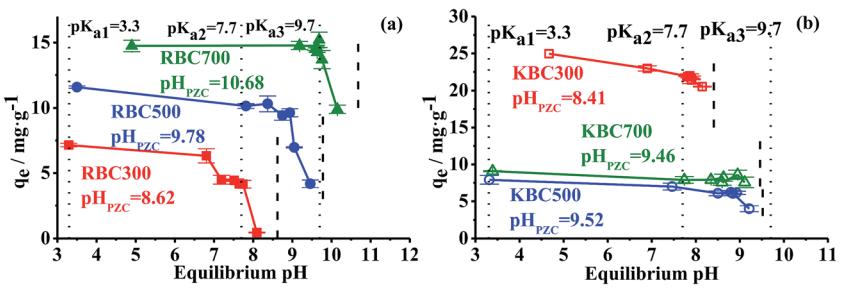

Fig. 6 Effect pH of solutions on the TC adsorption by RBCs (a) and KBCs (b). Initial concentration of TC: 30 mg L^{-1}; temperature: 298 K; initial pH = 3–9; ionic strength: 0.01 mol L^{-1} $NaNO_3$. Three pK_a of TC and PZC of biochars were labeled with vertical dot and dash lines.

was much lower than that for RBC300. This was consistent with promotion mechanism as above: n–π EDA interaction was stronger than other interactions such as hydrogen bonding due to electron displacement.[49] And high dissociation constant of –OH (pK_a > 10.25) would maintain proton to connect TC and biochars even in high pH.[36] On the contrary, q_e of KBC500 decreased when equilibrium pH reached to near pH_{PZC}, while q_e of KBC700 remained stable through different equilibrium pH. Due to less SOFGs left on KBC500 and KBC700, the extents of n–π EDA interaction, electrostatic attraction and H-bonding were reduced. Correspondingly, the adsorption mechanism of TC was dominated by cation–π bonding, which reduced the influence of pH_{eqm} (especially near pK_{a2}) on q_e. As such, the result suggested that KOH modification can enlarge the pH range of biochar for effective TC adsorption, especially for biochars from low pyrolysis temperatures.

4 Conclusion

The results of TC adsorptions by biochars from different pyrolysis temperatures and their KOH modified biochars indicated that the KOH modification process could either improve or inhibit TC adsorption under different conditions, which was mainly depended on changes of surface oxygen functional groups (SOFGs), not surface area. In this experiment, for the same modification conditions, KOH treatment increased SOFGs of biochars from low temperature (300 °C), and increased maximum adsorption capacities ($q_{e,m}$) in the kinetics adsorption experiment up to 21.17 mg g^{-1} from 4.30 mg g^{-1} of RBC300 (final TC concentration were 8.83 and 25.70 mg L^{-1}, respectively). Whereas, KOH treatment decreased SOFGs of biochars from the middle and high pyrolysis temperature range (500 and 700 °C) and TC adsorption amounts, even though their surface area was increased. A wide pH range for stable q_e can be found in modified biochars especially in biochar from pyrolysis temperature of 300 °C. Further analysis indicated the increase of acidic SOFGs such as –OH in KBC300 and strongly linear regression relationship between $q_{e,m}$ in the kinetics adsorption experiment and total surface functional oxygen groups ($n = 6$, $R^2 = 0.84$), whereas no significant relationship was found between $q_{e,m}$ and S_{BET} in this experiment.

Acknowledgements

This work was supported by (1) National Natural Science Foundation of China (41473070), (2) 863 Major Program (2013AA06A205), (3) The National Water Pollution Control and Treatment Science and Technology Major Project (2015ZX07203-011-06) (4) 863 achievement transformation program in Tianjin (No. 14RCHZSF00144), (5) Research Program of Application Foundation and Advanced Technology of Tianjin (No. 14JCYBJC43800).

References

1 M. Tripathi, J. N. Sahu and P. Ganesan, *Renewable Sustainable Energy Rev.*, 2016, **55**, 467–481.
2 J. Tang, W. Zhu, R. Kookana and A. Katayama, *J. Biosci. Bioeng.*, 2013, **116**, 653–659.
3 M. Ahmad, A. U. Rajapaksha, J. E. Lim, M. Zhang, N. Bolan, D. Mohan, M. Vithanage, S. S. Lee and Y. S. Ok, *Chemosphere*, 2014, **99**, 19–33.
4 L. Beesley, E. Moreno-Jimenez, J. L. Gomez-Eyles, E. Harris, B. Robinson and T. Sizmur, *Environ. Pollut.*, 2011, **159**, 3269–3282.
5 Y. Gao, Y. Li, L. Zhang, H. Huang, J. Hu, S. M. Shah and X. Su, *J. Colloid Interface Sci.*, 2012, **368**, 540–546.
6 K. G. Karthikeyan and M. T. Meyer, *Sci. Total Environ.*, 2006, **361**, 196–207.
7 A. K. Sarmah, M. T. Meyer and A. B. A. Boxall, *Chemosphere*, 2006, **65**, 725–759.
8 G. Li, W. Zhu, L. Zhu and X. Chai, *Korean J. Chem. Eng.*, 2016, **33**, 2215–2221.
9 P. Liu, W.-J. Liu, H. Jiang, J.-J. Chen, W.-W. Li and H.-Q. Yu, *Bioresour. Technol.*, 2012, **121**, 235–240.
10 D. N. Shan, S. B. Deng, T. N. Zhao, B. Wang, Y. J. Wang, J. Huang, G. Yu, J. Winglee and M. R. Wiesner, *J. Hazard. Mater.*, 2016, **305**, 156–163.
11 X. Zhu, Y. Liu, C. Zhou, G. Luo, S. Zhang and J. Chen, *Carbon*, 2014, **77**, 627–636.
12 M. B. Ahmed, J. L. Zhou, H. H. Ngo, W. Guo and M. Chen, *Bioresour. Technol.*, 2016, **214**, 836–851.
13 K. Sun, J. Tang, Y. Gong and H. Zhang, *Environ. Sci. Pollut. Res.*, 2015, **22**, 16640–16651.
14 L. Trakal, R. Šigut, H. Šillerová, D. Faturíková and M. Komárek, *Arabian J. Chem.*, 2014, **7**, 43–52.
15 P. Regmi, J. L. Garcia Moscoso, S. Kumar, X. Cao, J. Mao and G. Schafran, *J. Environ. Manage.*, 2012, **109**, 61–69.
16 H. Jin, S. Capareda, Z. Chang, J. Gao, Y. Xu and J. Zhang, *Bioresour. Technol.*, 2014, **169**, 622–629.
17 Y. Fan, B. Wang, S. Yuan, X. Wu, J. Chen and L. Wang, *Bioresour. Technol.*, 2010, **101**, 7661–7664.
18 C. Jung, J. Park, K. H. Lim, S. Park, J. Heo, N. Her, J. Oh, S. Yun and Y. Yoon, *J. Hazard. Mater.*, 2013, **263**(2), 702–710.
19 X.-R. Jing, Y.-Y. Wang, W.-J. Liu, Y.-K. Wang and H. Jiang, *Chem. Eng. J.*, 2014, **248**, 168–174.
20 J. J. Manya, *Environ. Sci. Technol.*, 2012, **46**, 7939–7954.
21 M. Keiluweit, P. S. Nico, M. G. Johnson and M. Kleber, *Environ. Sci. Technol.*, 2010, **44**, 1247–1253.
22 B. Chen, D. Zhou and L. Zhu, *Environ. Sci. Technol.*, 2008, **42**, 5137–5143.
23 W. E. Marshall and M. M. Johns, *J. Chem. Technol. Biotechnol.*, 1999, **66**, 192–198.
24 G. H. Oh and C. R. Park, *Fuel*, 2002, **81**, 327–336.
25 W. J. Braida, J. J. Pignatello, Y. Lu, P. I. Ravikovitch, A. V. Neimark and B. Xing, *Environ. Sci. Technol.*, 2003, **37**, 409–417.
26 S. Brunauer, P. H. Emmett and E. Teller, *J. Am. Chem. Soc.*, 1938, **60**, 309–319.
27 Y. Fan, X. Yang, B. Zhu, P.-F. Liu and H.-T. Lu, *J. Power Sources*, 2014, **268**, 584–590.
28 W.-J. Liu, F.-X. Zeng, H. Jiang and X.-S. Zhang, *Bioresour. Technol.*, 2011, **102**, 8247–8252.

29 H. P. Boehm, in *Advances in Catalysis*, ed. H. P. D. D. Eley and B. W. Paul, Academic Press, 1966, vol. 16, pp. 179–274.
30 S. L. Goertzen, K. D. Thériault, A. M. Oickle, A. C. Tarasuk and H. A. Andreas, *Carbon*, 2010, **48**, 1252–1261.
31 B. H. Hameed, I. A. W. Tan and A. L. Ahmad, *Chem. Eng. J.*, 2008, **144**, 235–244.
32 B. Chen and Z. Chen, *Chemosphere*, 2009, **76**, 127–133.
33 D. Angin, *Bioresour. Technol.*, 2013, **128**, 593–597.
34 P. Devi and A. K. Saroha, *Bioresour. Technol.*, 2015, **192**, 312–320.
35 P. Fu, W. Yi, X. Bai, Z. Li, S. Hu and J. Xiang, *Bioresour. Technol.*, 2011, **102**, 8211–8219.
36 Z. Chen, X. Xiao, B. Chen and L. Zhu, *Environ. Sci. Technol.*, 2015, **49**, 309–317.
37 M. Ahmad, S. S. Lee, A. U. Rajapaksha, M. Vithanage, M. Zhang, J. S. Cho, S. E. Lee and Y. S. Ok, *Bioresour. Technol.*, 2013, **143**, 615–622.
38 Y. Li, J. Shao, X. Wang, Y. Deng, H. Yang and H. Chen, *Energy Fuels*, 2014, **28**, 5119–5127.
39 S. Xin, H. Yang, Y. Chen, M. Yang, L. Chen, X. Wang and H. Chen, *J. Anal. Appl. Pyrolysis*, 2015, **116**, 263–271.
40 J. Zhang, J. Luo, D. Tong, L. Zhu, L. Dong and C. Hu, *Carbohydr. Polym.*, 2010, **79**, 164–169.
41 W. Tongpoothorn, M. Sriuttha, P. Homchan, S. Chanthai and C. Ruangviriyachai, *Chem. Eng. Res. Des.*, 2011, **89**, 335–340.
42 Y. S. Ho and G. McKay, *Process Biochem.*, 1999, **34**, 451–465.
43 A. C. Martins, O. Pezoti, A. L. Cazetta, K. C. Bedin, D. A. S. Yamazaki, G. F. G. Bandoch, T. Asefa, J. V. Visentainer and V. C. Almeida, *Chem. Eng. J.*, 2015, **260**, 291–299.
44 L. Zhou, Y. Liu, S. Liu, Y. Yin, G. Zeng, X. Tan, X. Hu, X. Hu, L. Jiang, Y. Ding, S. Liu and X. Huang, *Bioresour. Technol.*, 2016, **218**, 351–359.
45 X. Zhu, Y. Liu, F. Qian, C. Zhou, S. Zhang and J. Chen, *Bioresour. Technol.*, 2014, **154**, 209–214.
46 S. Sen Gupta and K. G. Bhattacharyya, *Adv. Colloid Interface Sci.*, 2011, **162**, 39–58.
47 J. Febrianto, A. N. Kosasih, J. Sunarso, Y.-H. Ju, N. Indraswati and S. Ismadji, *J. Hazard. Mater.*, 2009, **162**, 616–645.
48 V. Strelko Jr and D. J. Malik, *J. Colloid Interface Sci.*, 2002, **250**, 213–220.
49 L. Ji, W. Chen, L. Duan and D. Zhu, *Environ. Sci. Technol.*, 2009, **43**, 2322–2327.
50 D. Zhang, J. Yin, J. Zhao, H. Zhu and C. Wang, *J. Environ. Chem. Eng.*, 2015, **3**, 1504–1512.
51 F. Lian, Z. Song, Z. Liu, L. Zhu and B. Xing, *Environ. Pollut.*, 2013, **178**, 264–270.

